Search for β-delayed fission of ^{178}Au^{g,m} and an updated systematics in the region of neutron-deficient nuclei

B. Andel,[1,*] A. N. Andreyev,[2,3] S. Bara,[4] T. E. Cocolios,[4] J. G. Cubiss,[2,†] C. Page,[2] P. Van Duppen,[4] A. Algora,[5,6] S. Antalic,[1] M. Athanasakis-Kaklamanakis,[7] M. Au,[7] R. A. Bark,[8] A. Barzakh,[9] M. J. G. Borge,[10] A. Camaiani,[4,11,12] K. Chrysalidis,[7] C. Costache,[13] H. De Witte,[4] D. V. Fedorov,[9] V. N. Fedosseev,[7] L. M. Fraile,[14] H. O. U. Fynbo,[15] R. Grzywacz,[16] R. Heinke,[7] J. Johnson,[4] P. M. Jones,[8] D. S. Judson,[17] D. T. Kattikat Melcom,[18,‡] M. M. Khan,[4,19] J. Klimo,[4] A. Korgul,[20] M. Labiche,[21] R. Lică,[13] M. Madurga,[16] N. Marginean,[13] P. Marini,[18,‡] B. A. Marsh,[7,§] C. Mihai,[13] J. Mišt,[1] P. L. Molkanov,[9] E. Nácher,[5] C. Neacsu,[13] J. N. Orce,[22] R. D. Page,[17] J. Pakarinen,[23,24] P. Papadakis,[21] S. Pascu,[13] A. Perea,[10] M. Piersa-Siłkowska,[20] Zs. Podolyák,[25] C. Schmitt,[26] M. D. Seliverstov,[9] A. Sitarčík,[1] E. Stamati,[7,27] A. Stoica,[13] A. Stott,[2] M. Stryjczyk,[23,24,28] O. Tengblad,[10] I. Tsekhanovich,[18] A. Turturica,[13] J. M. Udías,[14] N. Warr,[29] and A. Youssef[4]
(IDS Collaboration)

[1]*Department of Nuclear Physics and Biophysics, Comenius University in Bratislava, 84248 Bratislava, Slovakia*
[2]*School of Physics, Engineering and Technology, University of York, York YO10 5DD, United Kingdom*
[3]*Advanced Science Research Center, Japan Atomic Energy Agency, Tokai-mura, Ibaraki 319-1195, Japan*
[4]*KU Leuven, Instituut voor Kern- en Stralingsfysica, B-3001 Leuven, Belgium*
[5]*Instituto de Física Corpuscular, CSIC-Universidad de Valencia, E-46071 Valencia, Spain*
[6]*Institute of Nuclear Research (ATOMKI), P.O. Box 51, H-4001 Debrecen, Hungary*
[7]*CERN, CH-1211 Geneve 23, Switzerland*
[8]*iThemba LABS, National Research Foundation, P.O. Box 722, Somerset West 7129, South Africa*
[9]*Affiliated with an institute covered by a cooperation agreement with CERN at the time of the experiment*
[10]*Instituto de Estructura de la Materia, CSIC, Serrano 113 bis, E-28006 Madrid, Spain*
[11]*Dipartimento di Fisica, Università di Firenze, I-50019 Sesto Fiorentino, Italy*
[12]*Istituto Nazionale di Fisica Nucleare, Sezione di Firenze, I-50019 Sesto Fiorentino, Italy*
[13]*"Horia Hulubei" National Institute for R & D in Physics and Nuclear Engineering, RO-077125 Bucharest, Romania*
[14]*Grupo de Física Nuclear and IPARCOS, Universidad Complutense de Madrid, CEI Moncloa, E-28040 Madrid, Spain*
[15]*Department of Physics and Astronomy, Aarhus University, DK-8000 Aarhus C, Denmark*
[16]*Department of Physics and Astronomy, University of Tennessee, Knoxville, Tennessee 37966, USA*
[17]*Oliver Lodge Laboratory, University of Liverpool, Liverpool L69 7ZE, United Kingdom*
[18]*Université de Bordeaux, CNRS, LP2I, UMR 5797, F-33170 Gradignan, France*
[19]*IMT Atlantique, Nantes Université, CNRS-IN2P33, Nantes, France*
[20]*Faculty of Physics, University of Warsaw, PL 02-093 Warsaw, Poland*
[21]*STFC Daresbury Laboratory, Daresbury, Warrington WA4 4AD, United Kingdom*
[22]*Department of Physics, University of the Western Cape, P/B X17 Bellville 7535, South Africa*
[23]*Accelerator Laboratory, Department of Physics, University of Jyväskylä, P.O. Box 35, FI-40014 Jyväskylä, Finland*
[24]*Helsinki Institute of Physics, University of Helsinki, FI-00014 Helsinki, Finland*
[25]*Department of Physics, University of Surrey, Guildford GU2 7XH, United Kingdom*
[26]*Institut Pluridisciplinaire Hubert Curien (IPHC), F-67000 Strasbourg, France*
[27]*University of Ioannina, P.O. Box 1186, Ioannina, Epirus, Greece*
[28]*Institut Laue-Langevin, 71 Avenue des Martyrs, F-38042 Grenoble, France*
[29]*Institut für Kernphysik, Universität zu Köln, D-50937 Köln, Germany*

(Received 25 August 2025; accepted 20 November 2025; published 26 January 2026)

*Contact author: boris.andel@fmph.uniba.sk
†Present address: School of Physics and Astronomy, University of Edinburgh, Edinburgh EH9 3FD, United Kingdom.
‡Present address: Grand Accélérateur National d'Ions Lourds, CNRS/IN2P3-CEA/DRF, 14000 Caen, France.
§Deceased.

A search for a β-delayed fission (βDF) decay branch of isomerically pure samples of ^{178}Au^{g} and ^{178}Au^{m} was performed at the ISOLDE-CERN facility. Two complementary detection systems capable of registering α decays and fission fragments, the ISOLDE Decay Station and the ASET (Alpha SETup), were used. Despite very high statistics of produced ^{178}Au nuclei, no fission fragments were detected. Upper limits of βDF probabilities of $P_{\beta\mathrm{DF}}(^{178}\mathrm{Au}^{g}) < 1.11(2) \times 10^{-8}$ and $P_{\beta\mathrm{DF}}(^{178}\mathrm{Au}^{m}) < 9.7(2) \times 10^{-9}$ were determined. Corresponding lower limits of βDF partial half-lives were deduced as well, and the results are discussed in the context of experimental systematics of βDF in the neutron-deficient region of the nuclear chart.

DOI: 10.1103/swd1-ydlm

I. INTRODUCTION

Beta-delayed fission (βDF) is a two-step process, where the mother nucleus first undergoes β decay into a state with an excitation energy close to the top of the fission barrier (B_f) in the daughter nucleus. The populated state then fissions in competition with other processes, such as γ-ray or particle emission. The probability of βDF can be theoretically expressed as

$$P_{\beta\mathrm{DF}} = \frac{\int_0^{Q_\beta} F(Q_\beta - E) S_\beta(E) \frac{\Gamma_f(E)}{\Gamma_{\mathrm{total}}(E)} dE}{\int_0^{Q_\beta} F(Q_\beta - E) S_\beta(E) dE}, \qquad (1)$$

where Q_β, $F(Q_\beta - E)$, and S_β are the Q value of β decay, the Fermi function, and β-strength function of the parent nucleus, respectively, E is the excitation energy, $\Gamma_f(E)$ is the fission decay width, and $\Gamma_{\mathrm{total}}(E)$ is the total decay width of the excited daughter nucleus; see, e.g., Refs. [1,2]. The fission decay width further depends on the fission barrier height, and the full expression for $\Gamma_f(E)$ can be found, for example, in Ref. [2].

As the achievable excitation energy of the daughter state is limited by the Q_β value of the mother nucleus, a $Q_\beta - B_f$ difference is a crucial parameter for the occurrence of βDF. Roughly exponential dependence of βDF probabilities and partial half-lives on the $Q_\beta - B_f$ parameter was observed in previous works [1,3]. Typically, Q_β values are $\lesssim$12 MeV in the neutron-deficient lead region and $\lesssim$6 MeV in the heavy actinides, thus βDF provides a unique opportunity to explore the so-called low-energy fission of nuclei far from the β-stability line. The term "low-energy" refers to the excitation energy of the fissioning system being below or moderately above the fission barrier. Such low excitation energy is crucial for the ability to study influence of shell effects and nuclear structure on the fission properties, such as fission fragment mass distributions (FFMDs) [1,4], or on the fission barrier height, which can be estimated based on βDF probability [2,5–7].

In the past years, βDF measurements were employed to study fission properties of many exotic isotopes in the neutron-deficient side of the nuclear chart, from the lead region up to the heavy actinides. Notably, an unexpected asymmetric fission of ^{180,178}Hg (βDF of ^{180,178}Tl) was observed [8–10], discovering a new region of asymmetric fission, and the evolution of FFMDs between mercury and radium was investigated [11]. These findings prompted strong interest from both theoretical and experimental teams. Various theoretical interpretations of the asymmetric fission in this region were proposed, for example shell effects in the compound system ^{180}Hg preventing fission fragments (prefragments) from entering a path in the potential energy surface leading to symmetric fission [12], coupling between specific levels resulting in presence of asymmetric saddle points in fission [13], or deformed shell gaps at quadrupole and octupole deformations in prefragments at scission [14,15]. Moreover, a calculation of fission yields for a large number of nuclei with $74 \leqslant Z \leqslant 94$ and $91 \leqslant Z \leqslant 150$ predicted a broader region of asymmetric fission located below lead [16].

Experimental efforts employed mainly fusion-fission measurements to investigate ^{180}Hg and neighboring nuclei, discovering a mixture of symmetric and asymmetric fission modes for many isotopes [17–25]. The dominant role of the protons in the light fission fragment (FF) was discussed in the first study of FF isotopic distributions in the preactinide region [21]. Moreover, theoretical analysis of available experimental results proposed that fission asymmetry in this region is mostly driven by the proton shell effects in the light FF, constraining its proton number to be around $Z_l \approx 36$ [26]. The general conclusions were supported by the following experiments [25], including large systematic studies mapping this new region of asymmetric fission, using the fusion-fission method [27] and electromagnetically induced fission [28].

While these approaches allow access to an impressive numbers of nuclei for large-statistics studies, βDF keeps the advantage of uniquely low excitation energies of the fissioning systems. In fusion-fission experiments, the excitation energies can reach down to $\gtrsim$30 MeV, but are often significantly higher [17–20,23–25]. For electromagnetically induced fission, the excitation energy is lower, but still typically $\approx$5–10 MeV above the top of the fission barrier [28].

Based on the systematics of βDF probabilities [3] and the $Q_\beta - B_f$ difference, the isotope ^{178}Au is a possible candidate for the occurrence of βDF in the new region of asymmetric fission. For example, for Q_β from the Atomic Mass Evaluation [29] and B_f from the finite-range liquid-drop model (FRLDM) [30], the difference is -3.1 MeV. This is comparable for instance to the $Q_\beta - B_f$ difference of -3.4 MeV for ^{246}Es, which has a known βDF decay branch [31]. We note that a combination of β^+ and electron capture (EC) decay occurs on the neutron-deficient side of the nuclear chart, but for simplicity we will refer to this combination as β decay, while Q_{EC} values will be used as Q_β.

The isotope ^{178}Pt, the β-decay daughter of ^{178}Au, was already investigated both by fusion-fission experiments [18,23,24] and by electromagnetically induced fission [28], revealing a mixture of symmetric and asymmetric fission modes in both types of measurements. However, obtaining FFMDs of ^{178}Pt from βDF of ^{178}Au is important to

expand the studies of the FFMD dependence on the excitation energy and to acquire a more complete picture of the region.

A further motivation for βDF study of ^{178}Au comes from the fact that it has two β-decaying states, with $I^\pi = (2^+, 3^-)$ and $I^\pi = (7^+, 8^-)$ [32,33], which from now on will be denoted as ^{178}Au^g and ^{178}Au^m, respectively. Since β decay dominantly populates levels with the same or similar spin and configuration as the initial state, separate βDF measurements of ^{178}Au^g and ^{178}Au^m would allow exploration of the poorly known spin dependence in fission. A similar experiment has been performed for ^{188}Bi^{g,m}, which has two β-decaying states with $I^\pi = (1^+)$ and $I^\pi = (10^-)$, respectively [34,35]. Despite limited statistics, the results hinted at a lower fission probability of low-spin states in the β-decay daughter, ^{188}Pb [34].

The present work reports on the search for βDF in the two β-decaying states in ^{178}Au performed at the ISOLDE facility at CERN [36,37]. The experiment and the employed detection systems are described in Sec. II. The analysis and results are presented in Sec. III, while Sec. IV discusses the results in relation to the βDF systematics.

II. EXPERIMENT

The ^{178}Au isotope was produced in proton-induced spallation reactions in a thick UC_x target (50 g/cm^2). A pulsed beam of 1.4-GeV protons was provided by the Proton Synchrotron Booster. The proton pulses were grouped into a so-called supercycle, containing typically around 30 pulses, part of which was delivered to the ISOLDE target. The maximum average proton beam intensity was up to 2 μA.

The produced isotopes diffused through the target material heated to ≈2300 K and effused into the hot cavity of the Resonance Ionization Laser Ion Source (RILIS) [39,40]. A three-step resonance ionization scheme using laser light with wavelengths of 267.6, 306.5, and 673.9 nm [41] was employed. The wave number of the first-step laser was set to selectively ionize either ^{178}Au^g or ^{178}Au^m. The separation of ^{178}Au^g and ^{178}Au^m hyperfine components is sufficiently large (see Fig. 1 of Ref. [33]) to achieve isomer selectivity already with a relatively broad linewidth of ≈9 GHz.[1] Thus, clean samples of a specific state were obtained without compromising ionization efficiency. The ions were extracted and accelerated by a 30-kV potential, and mass-separated by the General Purpose Separator according to their mass-to-charge ratio of $A/q = 178$.

The mass-separated ion beam was delivered to either the ISOLDE Decay Station (IDS) [42] or the Alpha SETup (ASET) [38,43]. In the IDS, the beam was implanted on a movable aluminized Mylar tape. In front of the implantation point, inside the box-shaped vacuum chamber, an array of six 7 × 7 mm^2 and one 15 × 15 mm^2 Hamamatsu silicon PIN diodes, shown in Fig. 1, was placed to detect α particles and FFs. A solar cell sensitive to FFs was also mounted on one side of the detector array, but was not used because of issues with electronic noise. Four high-purity germanium (HPGe) clover detectors for γ-ray detection, which were used to confirm the purity of the samples, were placed outside the vacuum chamber around the implantation position. The energy calibration of PIN diodes was performed using many α-decay lines from various isotopes produced also shortly before and after data taking for ^{178}Au; their full list is given in Ref. [44]. The energy resolution for α particles from the combined data from all seven PIN diodes was ≈27 keV (full width at half maximum, FWHM). The detection efficiency for α particles or a single FF was 3.8(4)%. More details on the energy calibration and efficiency determination can be found in the α- and γ-decay spectroscopy studies based on this data set in Refs. [44,45].

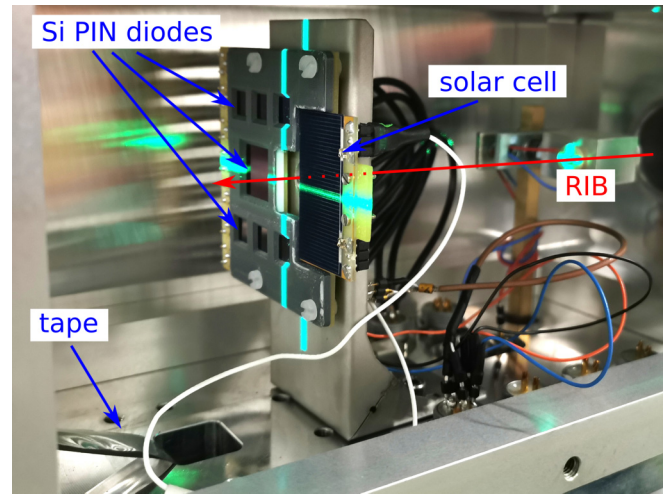

FIG. 1. An array of silicon PIN diodes used at the IDS. The tape is placed aside during the preparation of the system in the figure. During the measurement, the tape is mounted vertically in front of the detector array, where on top it is looped around a wheel and is moved parallel to the detectors. The red arrow (RIB) shows the direction of the radioactive ion beam passing through the hole in the detector mount.

In the ASET, the beam was implanted on one of nine thin carbon foils (20 μg/cm^2) mounted on a movable ladder. The implantation position was surrounded by two surface-barrier silicon detectors: an annular detector (Si1) upstream the beam and a full detector (Si2) downstream behind the foil, as shown in Fig. 2. The annular detector had a central hole with a diameter of 6 mm to let the beam pass through and its total area including the hole was 450 mm^2. The full detector had an area of 300 mm^2. A simple energy calibration was performed to align the spectra from separate data files, by using the known α-decay energies of 5446(3) keV for ^{178}Pt [46], 5922(5) keV for ^{178}Au^g, and 5925(7) keV for ^{178}Au^m [32]. The energy resolution for α particles for the whole data set was ≈200 keV for Si1 and ≈60–70 keV FWHM for Si2. The detection efficiencies for α particle or a single FF were estimated to be ≈15% for Si1 and ≈17% for Si2.

[1]The 267.6-nm wavelength is achieved by frequency tripling of Ti:Sa laser with a fundamental linewidth of 5 GHz [41]. The wave number before tripling was set to 12453.36 cm^{-1} for ^{178}Au^g and to 12454.02 cm^{-1} for ^{178}Au^m. After tripling, these wave numbers correspond to frequency shifts by 35 and 95 GHz, respectively, compared to arbitrarily chosen 0 position in the hyperfine structure spectrum in Fig. 1 of Ref. [33].

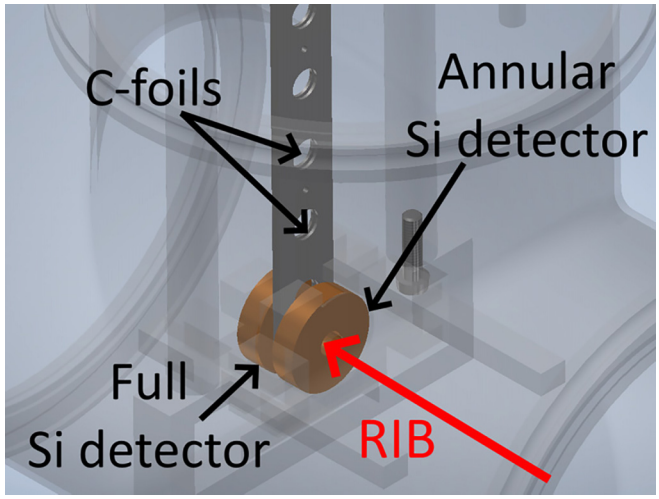

FIG. 2. ASET detection system. A ladder holding thin carbon foils (C-foils) is at the implantation position surrounded by two silicon detectors. The red arrow (RIB) shows the direction of the radioactive ion beam passing through the annular detector. The figure was taken from Ref. [38].

For the calibration at higher energies, where FFs can be expected, an extrapolation of the calibration based on α decays was used at both the IDS and ASET. Although the FF energies extracted in this way suffer from the pulse height defect (PHD) [47,48], the method is sufficient for identification of fission. For example, it was evaluated for βDF of ^{180}Tl that the average sum of energies of both FFs from a given event (total kinetic energy) determined using an extrapolated α energy calibration is only by ≈10 MeV lower compared to value of 133.2(14) MeV, which was corrected for PHD [10]. Therefore, FFs are still distinctly separated from α particles and are expected in the energy region of 40–90 MeV (see also, for example, Fig. 2 in Ref. [11]).

Most of the data were collected using low amplification gain to cover a broad energy range up to ≈160 MeV (IDS) and ≈100 MeV (ASET). The measurement of ^{178}Au^m with the IDS was an exception: most of the statistics (≈90%) listed in Table I for the IDS were collected using high amplification gain, covering energy only up to ≈40 MeV. However, the analog-to-digital converter (ADC) employed at the IDS provides a flag if a signal exceeds the ADC range.

III. RESULTS

A detailed α- and γ-decay spectroscopy analysis of the data set obtained with the IDS, which had better α-decay energy resolution and higher γ-ray detection efficiency than ASET, was performed in Refs. [44,45]. It confirmed isomer selectivity under the employed settings, as well as no sizable contamination of the beam by other isotopes.

TABLE I. Summary of obtained α-decay statistics for ^{178}Au^g and ^{178}Au^m, and total times of measurements at the IDS and ASET.

State	Setup	N_α	Time (h)
^{178}Au^g	IDS	$3.643(18)\times10^6$	≈18.6
	ASET	$9.28(7)\times10^6$	≈6.3
^{178}Au^m	IDS	$8.36(4)\times10^5$	≈5.8
	ASET	$1.564(13)\times10^7$	≈14.4

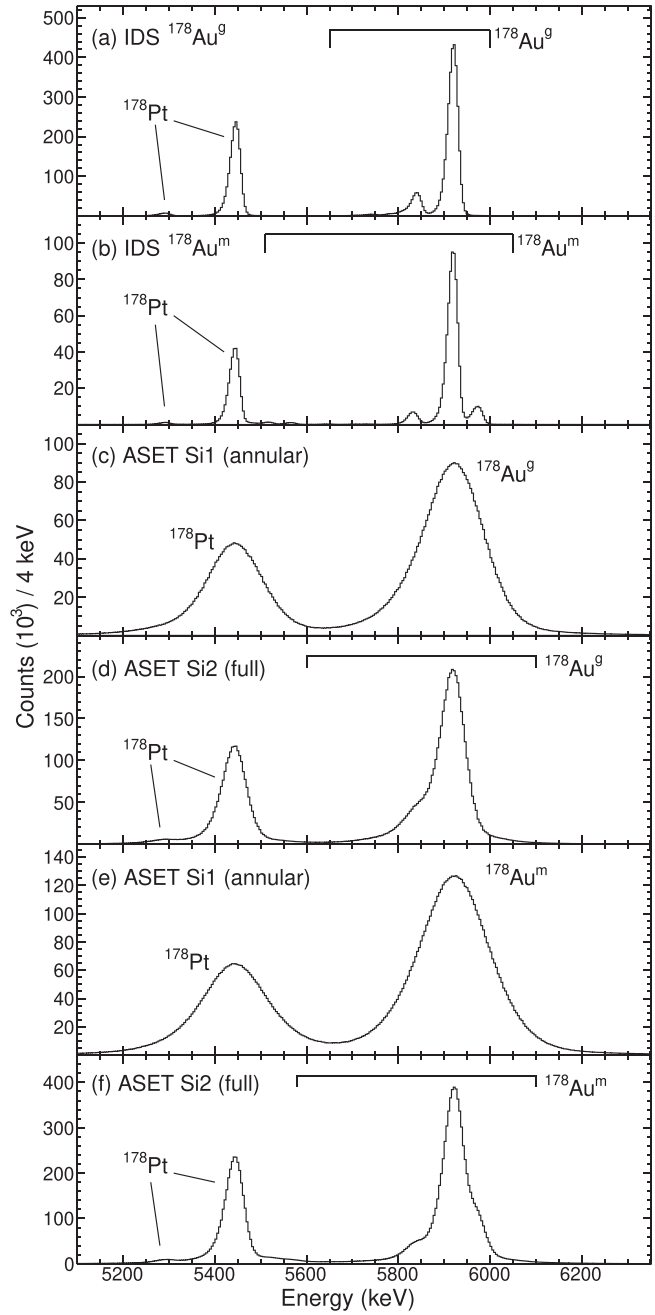

FIG. 3. α decays collected by (a) IDS PIN array for ^{178}Au^g, (b) IDS PIN array for ^{178}Au^m, (c) Si1 at ASET for ^{178}Au^g, (d) Si2 at ASET for ^{178}Au^g, (e) Si1 at ASET for ^{178}Au^m, and (f) Si2 at ASET for ^{178}Au^m. Isotope ^{178}Pt was produced only by β decay of ^{178}Au.

The summed α-decay spectra for the whole array of PIN diodes from the IDS are shown in Figs. 3(a) and 3(b). Most of the data for the βDF search were collected with ASET, because of its high α-decay and FF detection efficiency. All α decays registered at ASET are shown in Figs. 3(c), 3(d) for

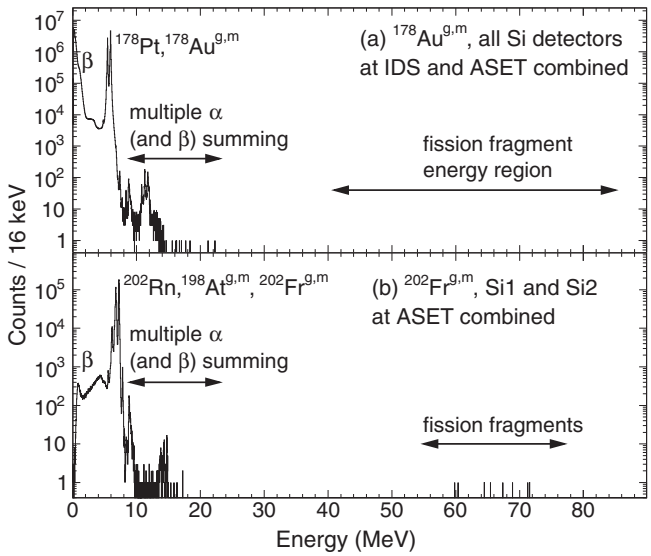

FIG. 4. Events from silicon detectors including higher-energy regions up to 90 MeV: (a) $^{178}Au^{g,m}$ measurements, all detectors from both the IDS and ASET combined, (b) ^{202}Fr test measurement at ASET, Si1 and Si2 combined. Isotopes ^{198}At and ^{202}Rn are α- and β-decay daughters of ^{202}Fr, respectively. In this type of experiment, FFs can typically be expected in the energy range of ≈40–90 MeV; see for example βDF events from higher-statistics measurement of ^{196}At in Fig. 2 in Ref. [11].

$^{178}Au^{g}$, and in Figs. 3(e), 3(f) for $^{178}Au^{m}$. The total α-decay statistics of $^{178}Au^{g,m}$ obtained with each detection system is given in Table I.

No FFs were detected during the measurement, as shown in Fig. 4(a). Similarly, in the high-gain mode data taken for $^{178}Au^{m}$ at IDS (Sec. II), no events exceeded the ADC range, and so these data were also included into the total α-decay statistics from both detection systems for $^{178}Au^{m}$. Upper limits of βDF probabilities and lower limits of βDF partial half-lives were determined. Experimentally, $P_{\beta DF}$ is defined as the ratio of the number of βDF events ($N_{\beta DF}$) to the number of β decays (N_β):

$$P_{\beta DF} = \frac{N_{\beta DF}}{N_\beta}. \tag{2}$$

However, α particles were registered in the present experiment, while the FFs would be measured by the same detectors. Thus, the upper limit of βDF probability is calculated as

$$P_{\beta DF} < \frac{N_{FF}}{2}\frac{b_\alpha}{N_\alpha(1-b_\alpha)}, \tag{3}$$

where N_α are the numbers of α decays of the βDF precursors $^{178}Au^{g,m}$, and b_α are their α-decay branching ratios $b_\alpha(^{178}Au^{g}) = 13.5(5)\%$ and $b_\alpha(^{178}Au^{m}) = 14.6(5)\%$ [45]. As the number of singles FFs, $N_{FF} = 1.84$ was used, which is an upper uncertainty for zero events from Poisson statistics with a confidence level of 84% [49]. Since the detection efficiencies of α particles or a single FF are the same, they cancel out in Eq. (3), and only a factor of $\frac{1}{2}$ remains, because two FFs are emitted in the fission process.[2] The deduced $P_{\beta DF}$ limits are $P_{\beta DF}(^{178}Au^{g}) < 1.11(2)\times10^{-8}$ and $P_{\beta DF}(^{178}Au^{m}) < 9.7(2)\times10^{-9}$.

The partial half-life of βDF can be deduced from the known $P_{\beta DF}$ value employing the following relation [50]:

$$T_{1/2p,\beta DF} = \frac{T_{1/2}}{b_\beta P_{\beta DF}}, \tag{4}$$

where $T_{1/2}$ and b_β are the half-life and β-decay branching ratio of the βDF precursor, respectively. Experimentally, $T_{1/2p,\beta DF}$ can be determined as [50]

$$T_{1/2p,\beta DF} = T_{1/2}\frac{N_{dec,tot}}{N_{\beta DF}}, \tag{5}$$

where $N_{dec,tot}$ is the total number of decays ($N_\alpha + N_\beta$) of the βDF precursor. If b_β is only estimated or uncertain, but expected to be $\leqslant$10%, an approximation $N_{dec,tot} \approx N_\alpha$ can be used [50]:

$$T_{1/2p,\beta DF} \approx T_{1/2}\frac{N_\alpha}{N_{\beta DF}}. \tag{6}$$

Using the same arguments and values as for the $P_{\beta DF}$ limit calculation in Eq. (3), the lower limits of βDF partial half-lives were determined by modifying Eq. (5) as follows:

$$T_{1/2p,\beta DF} > T_{1/2}\frac{2}{N_{FF}}\frac{N_\alpha}{b_\alpha}, \tag{7}$$

where $T_{1/2}$ are the half-lives of $^{178}Au^{g,m}$ from Ref. [45]. The resulting limits are $T_{1/2p,\beta DF}(^{178}Au^{g}) > 1.98(10)\times10^{8}$ s and $T_{1/2p,\beta DF}(^{178}Au^{m}) > 1.73(7)\times10^{8}$ s.

Similarly to our recent search for βDF in actinium isotopes [38], we performed a short measurement (≈70 min) with ^{202}Fr at ASET to test the system. This isotope has a known βDF decay branch with a partial βDF half-life of $T_{1/2p,\beta DF} = 4.6(8)\times10^{4}$ s (Table II), which was determined for the mixture of two β-decaying states produced at ISOLDE [50]. We observed 8 FFs, as shown in Fig. 4(b), and, using the same average $T_{1/2}$ and b_β as listed in Table II, we deduced the partial βDF half-life of $T_{1/2p,\beta DF} = 9.5(36)\times10^{4}$ s. The result is consistent with the mentioned reference value within 1.2σ, which confirms a normal operation of the ASET detection system. Because of the constraints on the available beam time, a similar ^{202}Fr test was not performed at the IDS.

[2]We note that when detecting singles FFs, the factor of $\frac{1}{2}$ in Eq. (3) is valid despite the 180° angle between the two FFs from a fission event. We may arbitrarily choose a hemisphere H1 covering 2π solid angle around the implantation foil. Out of all α particles, only one half will fly to H1. However, out of every fission event, exactly one FF will fly to H1, thus, all FFs flying to H1 are independent from each other and their angular distribution is isotropic. For a silicon detector placed in H1, the probability to detect a single FF from one fission event is then twice as high as the probability to detect an α particle from one α-decay event. The remaining FFs flying to the opposite hemisphere H2 are also independent from each other, so the same conclusions are also valid for H2. The total detection efficiency for fission events, when counting singles FFs, is then twice as high as the total detection efficiency for α particles.

TABLE II. βDF systematics on the neutron-deficient side of the nuclear chart including our limits for $^{178}Au^{g,m}$. The table contains the βDF precursor, its half-life ($T_{1/2}$); β-decay branching ratio (b_β); electron-capture decay Q values (Q_β) from AME 2020 [29]; $Q_\beta - B_f$ difference for fission barriers from the TF model [51] with microscopic corrections from FRDM [52], and for fission barriers from FRLDM [30]; probability of βDF ($P_{\beta\text{DF}}$), and partial half-life of βDF ($T_{1/2\text{p},\beta\text{DF}}$). The reference in the last column is relevant for $T_{1/2}$, b_β, $P_{\beta\text{DF}}$, and $T_{1/2\text{p},\beta\text{DF}}$ values in the given row, unless otherwise specified. Abbreviations "ls" and "hs" used for ^{188,190}Bi and ^{182}Tl stand for the low-spin and high-spin states, respectively.

				$Q_\beta - B_f$ (MeV)				
Precursor	$T_{1/2}$ (s)	b_β (%)	Q_β (MeV)	TF	FRLDM	$P_{\beta\text{DF}}$	$T_{1/2\text{p},\beta\text{DF}}$ (s)	Ref.
$^{178}Au^{g}$	3.81(12)[a]	86.5(5)[a]	9.69	−3.66	−3.13	$<1.11(2)\times10^{-8}$	$>1.98(10)\times10^{8}$	This work
$^{178}Au^{m}$	2.82(4)[a]	85.4(5)[a]	9.69	−3.66	−3.13	$<9.7(2)\times10^{-9}$	$>1.73(7)\times10^{8}$	This work
^{178}Tl	0.252(20)	38(2)	11.70	2.48	2.38	$1.5(6)\times10^{-3}$	$4.4(18)\times10^{2}$[b]	[10]
^{180}Tl	1.09(1)	94(4)	10.86	1.07	1.05	$3.2(2)\times10^{-5}$	$3.6(3)\times10^{4}$[b]	[8,9]
$^{182}Tl^{ls,hs}$	2.5(6)[c]	97.5(25)[d]	10.25	−0.41	−0.60	$<3.4\times10^{-8}$	$>5.2\times10^{7}$	[55]
$^{186}Bi^{g,m}$	0.012(3)[e]	≈0.6[f]	11.54	2.72	1.93	$\approx7.6\times10^{-2}$[g]	54(35)[h]	[58]
$^{188}Bi^{hs}$	0.250(10)[a]	≈1	10.62	0.82	0.30	$4.6(9)\times10^{-3}$	$5.6(8)\times10^{3}$	[34]
$^{188}Bi^{ls}$	0.060(3)[a]	≈2–8	10.62	0.82	0.30	$0.4(2)–1.8(7)\times10^{-3}$	$1.7(6)\times10^{3}$	[34]
$^{190}Bi^{hs}$	5.9(6)[a]	30(9)[a]	9.82	−1.18	−1.36		$\geqslant 4.7^{+22.6}_{-3.5}\times10^{7}$	[34]
$^{190}Bi^{ls}$	5.7(8)[a]	10^{+30}_{-10}[a]	9.82	−1.18	−1.36		$\geqslant 2.8^{+13.4}_{-2.1}\times10^{7}$	[34]
$^{192}At^{m1,m2}$	0.05(4)[e]	≈3[f]	10.99	4.08	2.74	≈0.19[i]	12(10)[h]	[59]
$^{194}At^{m1,m2}$	0.305(19)[j]	≈10[f]	10.29	2.33	0.83	8×10^{-3}[k]	$5.2(4)\times10^{2}$[h]	[11]
^{196}At	0.371(5)	2.5(3)	9.56	0.42	−0.73	$9(1)\times10^{-5}$	$1.6(3)\times10^{5}$[b]	[60]
^{200}Fr	0.0496(21)[l]	< 2.1[a]	10.13	3.04	1.52	$>3.1(17)\times10^{-2}$	$7^{+5}_{-3}\times10$[h]	[50]
$^{202}Fr^{g,m}$	0.33(4)[e]	2.4(2)[a]	9.38	0.85	−0.91	$3.0(4)\times10^{-4}$[m]	$4.6(8)\times10^{4}$[n]	[11,50]
^{228}Np	61.4(14)	60(7)	4.61	0.37	−0.52	$2.0(9)\times10^{-4}$	$5.1(24)\times10^{5}$[b]	[67]
^{230}Am	36^{+12}_{-7}	≈100	5.94	3.15	2.87	>0.3	$<1.2^{+0.4}_{-0.2}\times10^{2}$[b]	[3]
^{232}Am	78.6(24)	≈95[f]	5.06	1.71	1.83	$6.9(10)\times10^{-4}$	$1.20(18)\times10^{5}$[b]	[68]
^{234}Am	139(5)	≈100	4.11	0.08	0.28	$6.6(18)\times10^{-5}$	$2.1(6)\times10^{6}$[b]	[69]
^{236}Bk	22^{+13}_{-6}	≈100	5.69	2.63	1.88	0.04(2)	$5.5^{+4.3}_{-3.1}\times10^{2}$[b]	[70]
^{238}Bk	144(5)	≈100	4.77	1.05	−0.15	$4.8(20)\times10^{-4}$	$3.0(13)\times10^{5}$[b]	[71]
^{240}Bk	252(48)	≈100[f]	3.94	−0.21	−1.91	$1.3^{+1.8}_{-0.7}\times10^{-5}$	$1.9^{+2.3}_{-1.2}\times10^{7}$[b]	[5]
^{240}Es	6(2)	30(10)	6.24	3.04	1.02	0.16(6)	$1.3(8)\times10^{2}$[b]	[70]
^{242}Es	16.9(8)	58(2)[o]	5.41	1.69	−0.75	$1.5(4)\times10^{-2}$	$1.9(5)\times10^{3}$[b]	[72]
^{244}Es	37(4)[l]	96^{+2}_{-3}[l]	4.55	0.38	−2.14	$1.2(4)\times10^{-4}$	$3.2(11)\times10^{5}$[b]	[75]
^{246}Es	450(30)[l]	90.1(18)[l]	3.73	−0.83	−3.43	$3.7^{+8.5}_{-3.0}\times10^{-5}$	$1.4^{+5.8}_{-0.9}\times10^{7}$[b]	[31]
^{248}Es	$1.44(18)\times10^{3}$[l]	99.7(3)[l]	3.06	−1.92	−4.18	$3.5(18)\times10^{-6}$	$4.1(22)\times10^{8}$[b]	[31]
$^{246}Md^{m2}$	4.4(8)	>77	5.92	2.03	−0.21	>0.1	<57(10)[b]	[73]
^{250}Md	52(6)[l]	93(3)[l]	4.33	−0.52	−2.89	$2^{+2}_{-1}\times10^{-4}$	$2.8^{+2.8}_{-1.4}\times10^{5}$[b]	[76]

[a]Taken from Ref. [45] for $^{178}Au^{g,m}$, Ref. [53] for $^{188}Bi^{ls,hs}$ and $^{190}Bi^{ls,hs}$, and Ref. [54] for ^{200}Fr and $^{202}Fr^{g,m}$.
[b]Calculated according to Eq. (4) using the listed $T_{1/2}$, b_β, and $P_{\beta\text{DF}}$ values.
[c]Average of $T_{1/2}(^{182}Tl^{ls}) = 1.9(1)$ s [55] and evaluated $T_{1/2}(^{182}Tl^{hs}) = 3.1(10)$ s [56], with uncertainty taken as $|T^{hs}_{1/2} - T^{ls}_{1/2}|/2$.
[d]Taken from evaluation for the high-spin state [56]; for the low-spin state an upper limit of $b_\beta < 99.51\%$ was measured [55].
[e]Average of half-lives of the two states evaluated in systematics in Ref. [50].
[f]Calculated from ground-state theoretical partial half-lives of β and α decays from Ref. [57].
[g]Estimate for both βDF precursors from Ref. [58], assuming they both have $b_\beta \approx 0.6\%$.
[h]Calculated according to Eq. (6) using $N_{\beta\text{DF}}/N_\alpha$ (or $N_\alpha/N_{\beta\text{DF}}$) ratio from the original reference and the listed $T_{1/2}$.
[i]Average of estimates from Ref. [59] for the two states using various assumptions.
[j]Average of half-lives of the two states from Ref. [59], with uncertainty taken as $|T^{m2}_{1/2} - T^{m1}_{1/2}|/2$.
[k]Estimate for both βDF precursors from Ref. [59] assuming they both have $b_\beta \approx 8.3\%$.
[l]Taken from ENSDF evaluation: $A = 200$ [61], $A = 244$ [62], $A = 246$ [63], $A = 248$ [64], and $A = 250$ [65].
[m]Calculated using the listed $T_{1/2}$, b_β, and taking $N_{\beta\text{DF}}/N_\alpha = 7.3(8)\times10^{-6}$, which is the ratio from Ref. [50] multiplied by a factor of 10, since there was apparently a typographical error. Adjusted order of magnitude of the ratio is consistent with $T_{1/2\text{p},\beta\text{DF}}$ value from Ref. [50], and also with FF and α-decay rates given in Table 4.1 of the thesis based on the same data set [66].
[n]Calculated using the listed $T_{1/2}$, b_β, and taking $N_{\beta\text{DF}}/N_\alpha = 7.3(8)\times10^{-6}$[m].
[o]Average of values 59(3)% [72] and 57(3)% [73]. We note that the latter value was taken from the text of Ref. [73], the values in Table II and Fig. 8 of Ref. [73] are swapped with b_α [74].

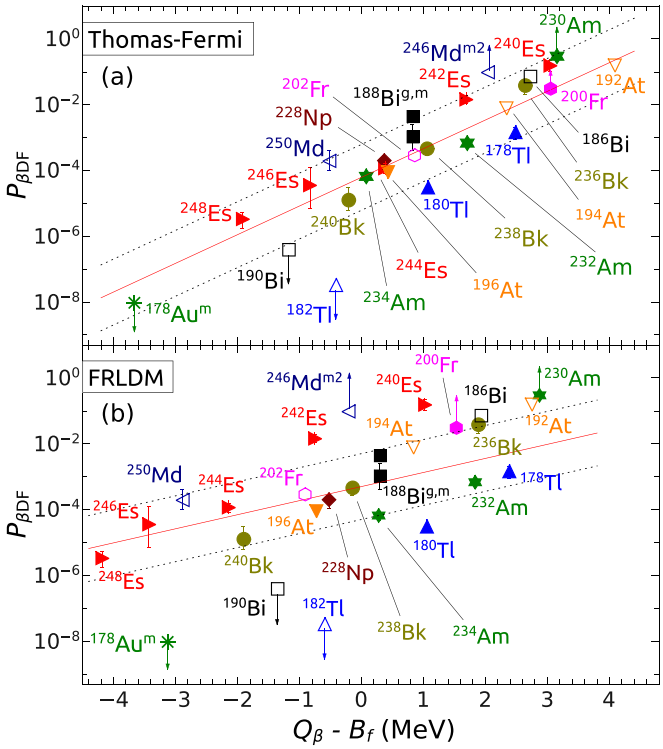

FIG. 5. Systematics of $P_{\beta DF}$ values in the neutron-deficient region as a function of difference $Q_\beta - B_f$ for B_f values (a) from the TF model [51] and (b) the FRLDM [30]. The plotted values are listed in Table II. Full symbols denote values (or limits) determined for a specific β-decaying state, while open symbols are used for estimates, where two different states could be precursors of βDF. Arrows indicate upper or lower limits. The red solid trend line is an exponential function, whose parameters were obtained by fitting the selected reliable points; see Table III and Sec. IV for details. The dotted lines use the same function, but are offset by ± one order of magnitude. We note that some data points are larger than the error bar range.

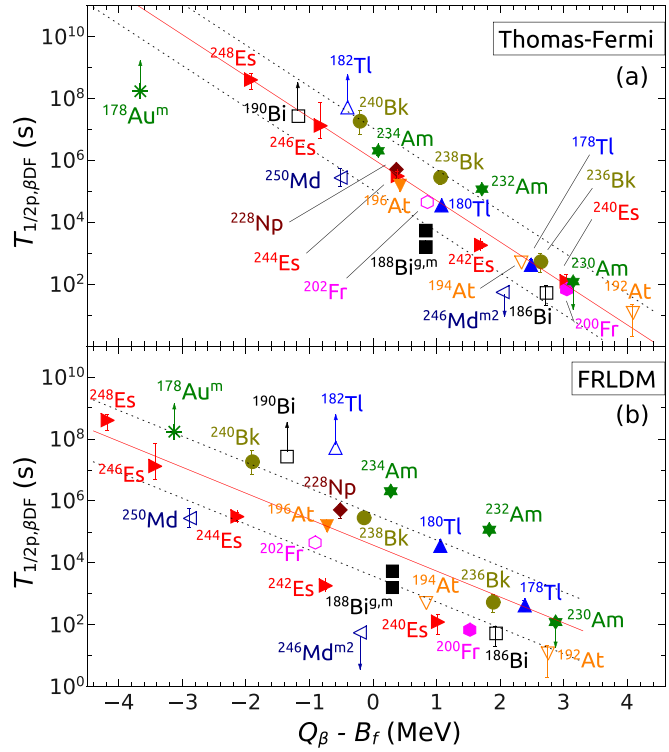

FIG. 6. The same as Fig. 5, but for partial half-lives of βDF.

IV. DISCUSSION

Updated βDF systematics for the neutron-deficient side of the nuclear chart, similar to one from a decade ago in Ref. [50], is compiled in Table II, including the $P_{\beta DF}$ and $T_{1/2p,\beta DF}$ limits for ^{178}Au^{g,m} from the present work. The listed $Q_\beta - B_f$ differences were calculated using fission barriers from two models: the FRLDM [30], and the Thomas-Fermi (TF) model [51] with microscopic corrections from the finite-range droplet model (FRDM) [52]. The experimental values from Table II are plotted as functions of $Q_\beta - B_f$ difference in Fig. 5 for $P_{\beta DF}$ and in Fig. 6 for $T_{1/2p,\beta DF}$. Since the limits for ^{178}Au^{g} and ^{178}Au^{m} are almost the same, only the limits for ^{178}Au^{m} are displayed in Figs. 5 and 6 to represent both states. Similarly, the limits for ^{190}Bi^{ls} [34] are displayed to represent both ^{190}Bi^{ls} and ^{190}Bi^{hs}.

The trend lines shown in Figs. 5 and 6 were constructed as functions $ae^{b(Q_\beta - B_f)}$, and their parameters are given in Table III. The parameters were obtained by fitting plots of $\ln(P_{\beta DF})$ and $\ln(T_{1/2p,\beta DF})$ values with a linear function $A + b(Q_\beta - B_f)$, using an unweighted least-squares fit. The parameter a is then equal to e^A. Limits, and data shown as open points in Figs. 5 and 6, denoting that two different states could be precursors of βDF, were excluded from the fits. In the case of $P_{\beta DF}$, the points for ^{188}Bi^{ls,hs} were also excluded, because their b_β are unknown and only small theoretical b_β values were used in determination of $P_{\beta DF}$, which introduces a large systematic uncertainty [34].

The systematics in Figs. 5 and 6 show the general trends recognized already in previous works [1,50], such as the exponential dependence of the $P_{\beta DF}$ and $T_{1/2p,\beta DF}$ values on the $Q_\beta - B_f$ difference, the overall shift to smaller $Q_\beta - B_f$ values for FRLDM-based systematics, and a smaller spread of values around the trend lines for TF-based plots compared to ones based on FRLDM fission barriers. The latter point is apparent also from the comparison of residual sums of squares per degree of freedom (RSS/NDF) in Table III. However, for

TABLE III. Parameters of trend lines $ae^{b(Q_\beta - B_f)}$ from Figs. 5 and 6. They were obtained by fitting plots of selected $\ln(P_{\beta DF})$ and $\ln(T_{1/2p,\beta DF})$ values with linear function $A + b(Q_\beta - B_f)$, using an unweighted least-squares fit, see Sec. IV for details. The parameter a is then equal to e^A. The last column contains residual sum of squares per degree of freedom from the fits.

Plot	B_f model	a	b	$\frac{\text{RSS}}{\text{NDF}}$
Fig. 5(a)	TF	$6.3(29)\times10^{-5}$	2.01(29)	2.1
Fig. 5(b)	FRLDM	$5.1(35)\times10^{-4}$	0.99(35)	6.3
Fig. 6(a)	TF	$1.1(6)\times10^{6}$	−3.09(32)	2.9
Fig. 6(b)	FRLDM	$3.7(26)\times10^{4}$	−1.93(38)	7.9

both models of the fission barriers, most of the experimental points fall within the range of ± one order of magnitude around the trend lines. Such a level of consistency can be considered satisfactory, when taking into account the spread over five and seven orders of magnitude for $P_{\beta\mathrm{DF}}$ and $T_{1/2\mathrm{p},\beta\mathrm{DF}}$ values, respectively (excluding those limits for which no βDF was observed).

It was discussed in Ref. [1] that different isotopic chains seem to have separate trend lines in FRLDM-based plots. However, only the einsteinium and berkelium isotopic chains have more than two reliable experimental points, and there is no known βDF case among gold isotopes. Thus, we also used only one common trend line for the FRLDM-based systematics in Figs. 5(b) and 6(b). Nevertheless, if the trend lines are determined only for the five einsteinium isotopes for either of the B_f models, the data points show almost perfect consistency with the exponential trend, resulting in RSS/NDF values between 0.4–1.3 [the lowest one comes from the fit of the $\ln(T_{1/2\mathrm{p},\beta\mathrm{DF}})$ plot based on the TF model].

The upper limit of $P_{\beta\mathrm{DF}} < 9.7(2) \times 10^{-9}$ deduced for $^{178}\mathrm{Au}^{m}$ is the lowest experimental value or limit measured on the neutron-deficient side of the nuclear chart (Fig. 5). Contrary to the general trend mentioned above, the $Q_\beta - B_f$ difference of −3.7 MeV for ^{178}Au based on the barrier from the TF model is lower than the −3.1 MeV difference based on FRLDM. As a result, the $P_{\beta\mathrm{DF}}$ limits for $^{178}\mathrm{Au}^{g,m}$ are roughly consistent with the trend of the TF-based systematics in Fig. 5(a), while there is a three-orders-of-magnitude deviation towards lower values in the FRLDM-based systematics in Fig. 5(b).

As it is apparent from Eqs. (3) and (7), upper limits of $P_{\beta\mathrm{DF}}$ translate to lower limits of $T_{1/2\mathrm{p},\beta\mathrm{DF}}$ shown in Fig. 6. In these systematics, the limit for ^{178}Au is roughly consistent with the trend when B_f values from the FRLDM are used [Fig. 6(b)]. However, when TF fission barriers are employed, the limit is more than two orders of magnitude below the trend line [Fig. 6(a)]. This leads to an interesting consequence: increasing statistics of measured α decays, while still not detecting βDF, will move the $T_{1/2\mathrm{p},\beta\mathrm{DF}}$ limit closer to the trend in the TF-based systematics in Fig. 6(a), but at the same time it will increase the inconsistency with $P_{\beta\mathrm{DF}}$ systematics within the same model in Fig. 5(a) as well as with both systematics based on FRLDM in Figs. 5(b) and 6(b).

For most other isotopes, both $P_{\beta\mathrm{DF}}$ and $T_{1/2\mathrm{p},\beta\mathrm{DF}}$ values are at the same time roughly consistent (or inconsistent) with the respective systematics in Figs. 5 and 6. In the case of inconsistency, it may be argued that the fission barrier height is different from the value predicted by a given model, and thus the inconsistency could be roughly resolved by shifting the point along the x axis in both the $P_{\beta\mathrm{DF}}$ and $T_{1/2\mathrm{p},\beta\mathrm{DF}}$ systematics. However, this is not the case for ^{178}Au since a shift along the x axis would improve the situation for $P_{\beta\mathrm{DF}}$ and worsen it for $T_{1/2\mathrm{p},\beta\mathrm{DF}}$ systematics, or vice versa.

The second lowest measured $P_{\beta\mathrm{DF}}$ is also only an upper limit of $P_{\beta\mathrm{DF}}(^{182}\mathrm{Tl}) < 3.4 \times 10^{-8}$, which was deduced for a mixture of two β-decaying states in ^{182}Tl based on absence of βDF events [55]. The corresponding lower limit of $T_{1/2\mathrm{p},\beta\mathrm{DF}}$ is $>5.2 \times 10^{7}$ s [55]. This isotope has a much larger $Q_\beta - B_f$ value compared to ^{178}Au (see Table II), thus the limits deviate from the trend lines even more strongly. The largest discrepancy, by ≈4 orders of magnitude, is for the FRLDM-based plot of $P_{\beta\mathrm{DF}}$ values in Fig. 5(b). Similarly to the ^{178}Au case, the discrepancies cannot be fully resolved by simply changing the fission barrier height, because for both models the inconsistency is much larger in the systematics of $P_{\beta\mathrm{DF}}$ values than in the $T_{1/2\mathrm{p},\beta\mathrm{DF}}$ systematics. Nevertheless, the limits for ^{182}Tl were determined for a mixture of two β-decaying states, and only a lower limit of the α-decay branching ratio of 0.49% for the low-spin state was deduced [55], which may contribute to the observed discrepancies.

Apart from the strong (exponential) $Q_\beta - B_f$ dependence, Eq. (1) shows that other parameters are crucial for the βDF probability. First of all, knowledge of the β-strength function S_β is needed for a more detailed discussion. The absence of βDF events in the ^{178}Au and ^{182}Tl measurements may have been caused by too weak or even nonexistent β-decay feeding to high-lying states. Moreover, level densities and pairing interaction in the daughter nucleus influence the fission decay width $\Gamma_f(E)$ [2]. As discussed, for example, in Ref. [70], the shape of the fission barrier is another important factor that can affect the $P_{\beta\mathrm{DF}}$ value. Therefore, the occurrence of βDF and its probability are a result of a complex interplay of various factors and the deeper discussion of the underlying physics is beyond the scope of the present study. Nevertheless, we note that dedicated experimental measurements of S_β, employing, for example, total absorption gamma spectroscopy [77], could strongly improve the understanding of $P_{\beta\mathrm{DF}}$ values.

V. CONCLUSIONS

Decay measurement using isomerically pure beams of $^{178}\mathrm{Au}^{g}$ and $^{178}\mathrm{Au}^{m}$ was performed at the ISOLDE-CERN facility with the aim to search for their β-delayed fission decay branch. Two complementary detection systems, the ISOLDE Decay Station (IDS) and Alpha SETup (ASET), were used.

More than 10^7 α decays for each state, $^{178}\mathrm{Au}^{g}$ and $^{178}\mathrm{Au}^{m}$, were detected, but no fission fragments were observed. Thus, upper limits of βDF probabilities were determined: $P_{\beta\mathrm{DF}}(^{178}\mathrm{Au}^{g}) < 1.11(2) \times 10^{-8}$ and $P_{\beta\mathrm{DF}}(^{178}\mathrm{Au}^{m}) < 9.7(2) \times 10^{-9}$. These limits are the lowest among all measured $P_{\beta\mathrm{DF}}$ values or limits on the neutron-deficient side of the nuclear chart. Lower limits of partial βDF half-lives, $T_{1/2\mathrm{p},\beta\mathrm{DF}}(^{178}\mathrm{Au}^{g}) > 1.98(10) \times 10^{8}$ s and $T_{1/2\mathrm{p},\beta\mathrm{DF}}(^{178}\mathrm{Au}^{m}) > 1.73(7) \times 10^{8}$ s, were also deduced.

The results were compared with the systematics of experimental values as functions of the $Q_\beta - B_f$ difference, where fission barrier heights B_f were taken from either the finite-range liquid-drop model (FRLDM) [30] or the Thomas-Fermi (TF) model [51]. The comparison showed large inconsistencies, mainly with the $P_{\beta\mathrm{DF}}$ plot using FRLDM fission barriers, and $T_{1/2\mathrm{p},\beta\mathrm{DF}}$ plot employing TF barriers. As a result, even within one given model, simply changing the fission barrier height or increasing the measured statistics will not lead to agreement with both the $P_{\beta\mathrm{DF}}$ and the $T_{1/2\mathrm{p},\beta\mathrm{DF}}$ systematics. The situation highlights the limitations of a simple picture using only the $Q_\beta - B_f$ difference as a key parameter, without considering other properties, for example the β-strength function.

ACKNOWLEDGMENTS

We acknowledge the support of the ISOLDE Collaboration and technical teams. This work was supported by the Slovak grant agency VEGA (Contract No. 1/0019/25), by the Slovak Research and Development Agency (Contracts No. APVV-18-0268 and No. APVV-22-0282), by the UK Science and Technology Facilities Council (Grants No. ST/P004598/1, No. ST/V001027/1, and No. ST/Y000242/1), by the FWO (Belgium) and F.R.S.-FNRS (Belgium) under the Excellence Of Science (EOS) program (Grants No. 30468642 and No. 40007501), by the Research Foundation Flanders under Projects No. I002619N, No. I002919N, and No. I012420N of the International Research Infrastructure, by the KU Leuven BOF (C14/22/104), by the FWO fellowship for fundamental research (Contract No. 1167324N), by the Spanish MCIN/AEI/10.13039/501100011033 under Grants No. PID2022-140162NB-I00, No. RTI2018-098868-B-I00, and No. PID2021-126998OB-I00, by Grupo de Fisica Nuclear (910059) at Universidad Complutense de Madrid, by the Polish Ministry of Science and Higher Education under Contract No. 2021/WK/07, by the Polish National Science Center under Grant No. 2020/39/B/ST2/02346, by the Romanian IFA grant CERN/ISOLDE and Nucleu Project No. PN 23 21 01 02, and by the German BMBF under Contract No. 05P21PKCI1 and BMBF Verbundprojekt 05P2021. M. Stryjczyk, acknowledges funding from the European Union's Horizon 2020 research and innovation programme under Grant Agreement No. 771036 (ERC CoG MAIDEN).

DATA AVAILABILITY

The data that support the findings of this article are not publicly available. The data are available from the authors upon reasonable request.

[1] A. N. Andreyev, M. Huyse, and P. Van Duppen, Rev. Mod. Phys. **85**, 1541 (2013).

[2] M. Veselský, A. N. Andreyev, S. Antalic, M. Huyse, P. Möller, K. Nishio, A. J. Sierk, P. Van Duppen, and M. Venhart, Phys. Rev. C **86**, 024308 (2012).

[3] G. L. Wilson, M. Takeyama, A. N. Andreyev, B. Andel, S. Antalic, W. N. Catford, L. Ghys, H. Haba, F. P. Heßberger, M. Huang, *et al.*, Phys. Rev. C **96**, 044315 (2017).

[4] A. N. Andreyev, K. Nishio, and K.-H. Schmidt, Rep. Prog. Phys. **81**, 016301 (2018).

[5] D. Galeriu, J. Phys. G: Nucl. Phys. **9**, 309 (1983).

[6] D. Habs, H. Klewe-Nebenius, V. Metag, B. Neumann, and H. J. Specht, Z. Phys. A **285**, 53 (1978).

[7] H. V. Klapdor, C.-O. Wene, I. N. Isosimov, and Y. W. Naumow, Z. Phys. A **292**, 249 (1979).

[8] A. N. Andreyev, J. Elseviers, M. Huyse, P. Van Duppen, S. Antalic, A. Barzakh, N. Bree, T. E. Cocolios, V. F. Comas, J. Diriken, D. Fedorov, *et al.*, Phys. Rev. Lett. **105**, 252502 (2010).

[9] J. Elseviers, A. N. Andreyev, M. Huyse, P. Van Duppen, S. Antalic, A. Barzakh, N. Bree, T. E. Cocolios, V. F. Comas, J. Diriken, D. Fedorov, *et al.*, Phys. Rev. C **88**, 044321 (2013).

[10] V. Liberati, A. N. Andreyev, S. Antalic, A. Barzakh, T. E. Cocolios, J. Elseviers, D. Fedorov, V. N. Fedoseeev, M. Huyse, D. T. Joss, *et al.*, Phys. Rev. C **88**, 044322 (2013).

[11] L. Ghys, A. N. Andreyev, M. Huyse, P. Van Duppen, S. Sels, B. Andel, S. Antalic, A. Barzakh, L. Capponi, T. E. Cocolios, *et al.*, Phys. Rev. C **90**, 041301(R) (2014).

[12] T. Ichikawa, A. Iwamoto, P. Möller, and A. J. Sierk, Phys. Rev. C **86**, 024610 (2012).

[13] T. Ichikawa and P. Möller, Phys. Lett. B **789**, 679 (2019).

[14] G. Scamps and C. Simenel, Nature (London) **564**, 382 (2018).

[15] G. Scamps and C. Simenel, Phys. Rev. C **100**, 041602(R) (2019).

[16] P. Möller and J. Randrup, Phys. Rev. C **91**, 044316 (2015).

[17] K. Nishio, A. N. Andreyev, R. Chapman, X. Derkx, C. E. Düllmann, L. Ghys, F. P. Heßberger, K. Hirose, H. Ikezoe, J. Khuyagbaatar, *et al.*, Phys. Lett. B **748**, 89 (2015).

[18] I. Tsekhanovich, A. N. Andreyev, K. Nishio, D. Denis-Petit, K. Hirose, H. Makii, Z. Matheson, K. Morimoto, K. Morita, W. Nazarewicz, *et al.*, Phys. Lett. B **790**, 583 (2019).

[19] E. Prasad, D. J. Hinde, M. Dasgupta, D. Y. Jeung, A. C. Berriman, B. M. A. Swinton-Bland, C. Simenel, E. C. Simpson, R. Bernard, E. Williams, *et al.*, Phys. Lett. B **811**, 135941 (2020).

[20] A. A. Bogachev, E. M. Kozulin, G. N. Knyazheva, I. M. Itkis, M. G. Itkis, K. V. Novikov, D. Kumar, T. Banerjee, I. N. Diatlov, M. Cheralu, *et al.*, Phys. Rev. C **104**, 024623 (2021).

[21] C. Schmitt, A. Lemasson, K.-H. Schmidt, A. Jhingan, S. Biswas, Y. H. Kim, D. Ramos, A. N. Andreyev, D. Curien, M. Ciemala, *et al.*, Phys. Rev. Lett. **126**, 132502 (2021).

[22] A. Jhingan, C. Schmitt, A. Lemasson, S. Biswas, Y. H. Kim, D. Ramos, A. N. Andreyev, D. Curien, M. Ciemała, E. Clément, *et al.*, Phys. Rev. C **106**, 044607 (2022).

[23] E. M. Kozulin, G. N. Knyazheva, I. M. Itkis, M. G. Itkis, Y. S. Mukhamejanov, A. A. Bogachev, K. V. Novikov, V. V. Kirakosyan, D. Kumar, T. Banerjee, *et al.*, Phys. Rev. C **105**, 014607 (2022).

[24] B. M. A. Swinton-Bland, J. Buete, D. J. Hinde, M. Dasgupta, T. Tanaka, A. C. Berriman, D. Y. Jeung, K. Banerjee, L. T. Bezzina, I. P. Carter, *et al.*, Phys. Lett. B **837**, 137655 (2023).

[25] H. R. Duan, H. M. Jia, C. J. Lin, D. J. Hinde, K. Banerjee, J. Buete, I. P. Carter, K. J. Cook, M. Dasgupta, C. Sengupta, *et al.*, Phys. Rev. C **111**, 044613 (2025).

[26] K. Mahata, C. Schmitt, S. Gupta, A. Shrivastava, G. Scamps, and K.-H. Schmidt, Phys. Lett. B **825**, 136859 (2022).

[27] J. Buete, B. M. A. Swinton-Bland, D. J. Hinde, K. J. Cook, M. Dasgupta, A. C. Berriman, D. Y. Jeung, K. Banerjee, L. T. Bezzina, I. P. Carter, *et al.*, Phys. Lett. B **865**, 139459 (2025).

[28] P. Morfouace, J. Taieb, A. Chatillon, L. Audouin, G. Blanchon, R. N. Bernard, N. Dubray, N. Pillet, D. Regnier, H. Alvarez-Pol, *et al.*, Nature (London) **641**, 339 (2025).

[29] M. Wang, W. J. Huang, F. G. Kondev, G. Audi, and S. Naimi, Chin. Phys. C **45**, 030003 (2021).
[30] P. Möller, A. J. Sierk, T. Ichikawa, A. Iwamoto, and M. Mumpower, Phys. Rev. C **91**, 024310 (2015).
[31] D. A. Shaughnessy, K. E. Gregorich, M. R. Lane, C. A. Laue, D. M. Lee, C. A. McGrath, D. A. Strellis, E. R. Sylwester, P. A. Wilk, and D. C. Hoffman, Phys. Rev. C **63**, 037603 (2001).
[32] J. G. Cubiss, A. N. Andreyev, A. Barzakh, V. Manea, M. Al Monthery, N. A. Althubiti, B. Andel, S. Antalic, D. Atanasov, K. Blaum, *et al.*, Phys. Rev. C **102**, 044332 (2020).
[33] J. G. Cubiss, A. N. Andreyev, A. E. Barzakh, P. Van Duppen, S. Hilaire, S. Péru, S. Goriely, M. Al Monthery, N. A. Althubiti, B. Andel, *et al.*, Phys. Rev. Lett. **131**, 202501 (2023).
[34] B. Andel, A. N. Andreyev, S. Antalic, M. Al Monthery, A. Barzakh, M. L. Bissell, K. Chrysalidis, T. E. Cocolios, J. G. Cubiss, T. Day Goodacre, *et al.*, Phys. Rev. C **102**, 014319 (2020).
[35] A. Barzakh, A. N. Andreyev, C. Raison, J. G. Cubiss, P. Van Duppen, S. Péru, S. Hilaire, S. Goriely, B. Andel, S. Antalic, *et al.*, Phys. Rev. Lett. **127**, 192501 (2021).
[36] R. Catherall, W. Andreazza, M. Breitenfeldt, A. Dorsival, G. J. Focker, T. P. Gharsa, T. J. Giles, J.-L. Grenard, F. Locci, P. Martins, *et al.*, J. Phys. G: Nucl. Part. Phys. **44**, 094002 (2017).
[37] E. Kugler, Hyperfine Interact. **129**, 23 (2000).
[38] S. Bara, A. Algora, B. Andel, A. N. Andreyev, S. Antalic, R. A. Bark, M. J. G. Borge, A. Camaiani, T. E. Cocolios, J. G. Cubiss, *et al.*, Phys. Rev. C **111**, 065803 (2025).
[39] V. Fedosseev, K. Chrysalidis, T. Day Goodacre, B. Marsh, S. Rothe, C. Seiffert, and K. Wendt, J. Phys. G: Nucl. Part. Phys. **44**, 084006 (2017).
[40] V. N. Fedoseyev, G. Huber, U. Köster, J. Lettry, V. I. Mishin, H. Ravn, V. Sebastian, and the ISOLDE Collaboration, Hyperfine Interact. **127**, 409 (2000).
[41] S. Rothe, T. Day Goodacre, D. V. Fedorov, V. N. Fedosseev, B. A. Marsh, P. L. Molkanov, R. E. Rossel, M. D. Seliverstov, M. Veinhard, and K. D. A. Wendt, Nucl. Instrum. Methods Phys. Res., Sect. B **376**, 91 (2016).
[42] ISOLDE Decay Station, https://isolde-ids.web.cern.ch/
[43] S. Bara, E. Jajčišinová, T. E. Cocolios, B. Andel, S. Antalic, A. Camaiani, C. Costache, K. Dockx, G. J. Farooq-Smith, A. Kellerbauer, *et al.*, Appl. Radiat. Isot. **208**, 111289 (2024).
[44] C. A. A. Page, Ph.D. thesis, University of York, United Kingdom, 2025 (unpublished), https://etheses.whiterose.ac.uk/id/eprint/36904/
[45] C. Page, A. N. Andreyev, S. Antalic, A. Barzakh, *et al.* (unpublished).
[46] A. Rytz, At. Data Nucl. Data Tables **47**, 205 (1991).
[47] H. W. Schmitt, W. E. Kiker, and C. W. Williams, Phys. Rev. **137**, B837 (1965).
[48] E. Weissenberger, P. Geltenbort, A. Oed, F. Gönnenwein, and H. Faust, Nucl. Instrum. Methods Phys. Res., Sect. A **248**, 506 (1986).
[49] K.-H. Schmidt, C.-C. Sahm, K. Pielenz, and H.-G. Clerc, Z. Phys. A **316**, 19 (1984).
[50] L. Ghys, A. N. Andreyev, S. Antalic, M. Huyse, and P. Van Duppen, Phys. Rev. C **91**, 044314 (2015).
[51] W. D. Myers and W. J. Świątecki, Phys. Rev. C **60**, 014606 (1999).
[52] P. Möller, A. J. Sierk, T. Ichikawa, and H. Sagawa, At. Data Nucl. Data Tables **109-110**, 1 (2016).
[53] A. N. Andreyev, D. Ackermann, S. Antalic, H. J. Boardman, P. Cagarda, J. Gerl, F. P. Heßberger, S. Hofmann, M. Huyse, D. Karlgren, *et al.*, Eur. Phys. J. A **18**, 39 (2003).
[54] L. Ghys, A. N. Andreyev, M. Huyse, P. Van Duppen, S. Antalic, A. Barzakh, L. Capponi, T. E. Cocolios, J. Cubiss, X. Derkx, *et al.*, Phys. Rev. C **100**, 054310 (2019).
[55] C. Van Beveren, A. N. Andreyev, A. E. Barzakh, T. E. Cocolios, R. P. de Groote, D. Fedorov, V. N. Fedosseev, R. Ferrer, L. Ghys, M. Huyse, *et al.*, J. Phys. G: Nucl. Part. Phys. **43**, 025102 (2016).
[56] B. Singh, Nucl. Data Sheets **130**, 21 (2015).
[57] P. Möller, M. Mumpower, T. Kawano, and W. D. Myers, At. Data Nucl. Data Tables **125**, 1 (2019).
[58] J. F. W. Lane, A. N. Andreyev, S. Antalic, D. Ackermann, J. Gerl, F. P. Heßberger, S. Hofmann, M. Huyse, H. Kettunen, A. Kleinböhl, *et al.*, Phys. Rev. C **87**, 014318 (2013).
[59] A. N. Andreyev, S. Antalic, D. Ackermann, L. Bianco, S. Franchoo, S. Heinz, F. P. Heßberger, S. Hofmann, M. Huyse, Z. Kalaninová, *et al.*, Phys. Rev. C **87**, 014317 (2013).
[60] V. L. Truesdale, A. N. Andreyev, L. Ghys, M. Huyse, P. Van Duppen, S. Sels, B. Andel, S. Antalic, A. Barzakh, L. Capponi, *et al.*, Phys. Rev. C **94**, 034308 (2016).
[61] F. G. Kondev, Nucl. Data Sheets **192**, 1 (2023).
[62] C. D. Nesaraja, Nucl. Data Sheets **146**, 387 (2017).
[63] C. D. Nesaraja, Nucl. Data Sheets **198**, 449 (2024).
[64] M. J. Martin, Nucl. Data Sheets **122**, 377 (2014).
[65] Y. A. Akovali, Nucl. Data Sheets **94**, 131 (2001).
[66] L. Ghys, Ph.D. thesis, KU Leuven, Belgium, 2015 (unpublished), https://fys.kuleuven.be/iks/ns/files/thesis/thesisprintfinal-lars.pdf
[67] S. A. Kreek, H. L. Hall, K. E. Gregorich, R. A. Henderson, J. D. Leyba, K. R. Czerwinski, B. Kadkhodayan, M. P. Neu, C. D. Kacher, T. M. Hamilton, *et al.*, Phys. Rev. C **50**, 2288 (1994).
[68] H. L. Hall, K. E. Gregorich, R. A. Henderson, C. M. Gannett, R. B. Chadwick, J. D. Leyba, K. R. Czerwinski, B. Kadkhodayan, S. A. Kreek, N. J. Hannink, *et al.*, Phys. Rev. C **42**, 1480 (1990).
[69] H. L. Hall, K. E. Gregorich, R. A. Henderson, C. M. Gannett, R. B. Chadwick, J. D. Leyba, K. R. Czerwinski, B. Kadkhodayan, S. A. Kreek, D. M. Lee, *et al.*, Phys. Rev. C **41**, 618 (1990).
[70] J. Konki, J. Khuyagbaatar, J. Uusitalo, P. T. Greenlees, K. Auranen, H. Badran, M. Block, R. Briselet, D. M. Cox, M. Dasgupta, *et al.*, Phys. Lett. B **764**, 265 (2017).
[71] S. A. Kreek, H. L. Hall, K. E. Gregorich, R. A. Henderson, J. D. Leyba, K. R. Czerwinski, B. Kadkhodayan, M. P. Neu, C. D. Kacher, T. M. Hamilton, *et al.*, Phys. Rev. C **49**, 1859 (1994).
[72] J. Khuyagbaatar, R. A. Cantemir, Ch. E. Düllmann, E. Jäger, B. Kindler, J. Krier, N. Kurz, B. Lommel, B. Schausten, and A. Yakushev, Phys. Rev. C **109**, 034311 (2024).
[73] S. Antalic, F. P. Heßberger, S. Hofmann, D. Ackermann, S. Heinz, B. Kindler, I. Kojouharov, P. Kuusiniemi, M. Leino, B. Lommel, R. Mann, and Š. Šáro, Eur. Phys. J. A **43**, 35 (2010).
[74] S. Antalic (private communication).

[75] D. A. Shaughnessy, K. E. Gregorich, J. L. Adams, M. R. Lane, C. A. Laue, D. M. Lee, C. A. McGrath, V. Ninov, J. B. Patin, D. A. Strellis, E. R. Sylwester, P. A. Wilk, and D. C. Hoffman, Phys. Rev. C **65**, 024612 (2002).

[76] Y. P. Gangrsky, G. M. Marinesky, M. B. Miller, V. N. Samsuk, and I. F. Kharisov, Yad. Fiz. **27**, 894 (1978) [Sov. J. Nucl. Phys. **27**, 475 (1978)].

[77] A. Algora, J. L. Tain, B. Rubio, M. Fallot, and W. Gelletly, Eur. Phys. J. A **57**, 85 (2021).